MULTIFREQUENCY RADIOMETRIC METHOD OF THE TEMPERATURE PROFILE MEASUREMENT IN THE ACTIVE TOPSOIL

K. V. Muzalevskiy,[*] **Z. Ruzhecka, and V. L. Mironov**   UDC 537.86

In this theoretical paper, we propose a method for measuring the temperature profile in the active topsoil of the Arctic tundra using observations of the brightness temperature for two different polarizations of the radiation at frequencies of 1.4, 6.93, 7.3, and 10.7 GHz. A multifrequency physical model of microwave emission of bare soil, a dielectric model of the Arctic tundra soil, and temperature profiles, which were measured in the active topsoil at the Toolik field station on the Alaska North Slope, were used to calculate the observed values of the brightness temperature. Temperature profiles were retrieved from the observed values of the brightness temperature in the approximation of a piecewise-linear profile of topsoil temperature during 2010–2011. Correlation analysis of the temperature profiles measured at the Toolik station and retrieved from the radiometric data has shown that in winter the error of measurement of the soil temperature at depths of 0.6 and 16.0 cm in terms of the variance (correlation coefficient) does not exceed 2.3 (0.98) and 7.2 (0.62°C), respectively. In summer, the error of measurement of the soil temperature using the radiometric method is two times less than in winter.

1. INTRODUCTION

The topsoil temperature reflects integrated changes in the energy balance between the atmosphere and the permafrost regions during the global change in the Earth's weather. Currently, the topsoil temperature in the Arctic region is measured using a spatially distributed, strongly rarefied network of weather stations. The small number of such stations limits significantly the capabilities of monitoring of the Arctic topsoil temperature mode and does not provide the required amount of input data for climatic models. Radiometric measurements in the microwave and infrared wavelength using remote-sensing satellites are sensitive to dryland temperature, have a high spatial resolution, cover a major part of the Arctic surface, and can be an effective tool to complement the small amount of surface data.

The most significant results of measuring the topsoil temperature in the permafrost area by radiometers were published in [1, 2]. In [1], the topsoil temperature of the grass–shrubby tundra on the territory of the Alaska North Slope (USA) and the Province of Quebec (Canada) was retrieved from the MODIS radiometer data of the Terra and Aqua satellites in the infrared wavelength range. It was found that in all sessions from year 2000 to year 2008 the standard deviation of the retrieved soil temperature from the value measured at the weather station at a depth of 3 to 5 cm was 7.7°C, and the corresponding correlation coefficient was 0.90. The soil temperature has not been retrieved in more than 40% of the cases because of the strong effect of clouds.

[*] rsdkm@ksc.krasn.ru

Compared with the infrared waves, the micro waves have a greater penetrating power through the snow and vegetation cover, and are also subject to a much smaller impact of such weather conditions as precipitation, cloudiness, etc. The authors of [2] study the possibility of measuring the Arctic tundra soil temperature using the AMSR-E radiometer of the Aqua satellite in a frequency range of 6.9 to 89.0 GHz. The proposed method is based on the solution of the radiometric equation (which allows for the vegetation and snow cover) with respect to the effective soil temperature, assuming a homogeneous isothermal soil layer. The retrieved depth profile of the soil temperature correlated with the profile in a layer 5 cm thick, which was *in situ* measured by weather stations. Depending on the choice of the test areas on the Alaska North Slope, the standard deviation of the retrieved soil temperature from the true value varied from 9.2 to 10.5°C and the correlation coefficient, from 0.6 to 0.8, respectively. In [2], the considerable errors of the soil temperature retrieval were attributed to the effect of large gradients of the temperature and dielectric permittivity in the active topsoil.

In [3], on the basis of radiometric multifrequency measurements at wavelengths of 0.8, 3, 9, and 13 cm we retrieved the subsurface temperature profiles and the evolution of the soil surface temperature and also estimated the humidity, temperature conductivity, complex dielectric permittivity, and the freezing depth of the mineral soil. Integral equations for the subsurface soil temperature were obtained and a method for the temperature profile retrieval with the emitting soil surface shielded was developed. In the equations relating the brightness temperature and the soil temperature profile, the reflection coefficient was assumed equal to zero. Owing to this, the temperature profile and temperature dependence of the dielectric permittivity of the topsoil, as well as the unevenness of the air–soil interface, were neglected in the radiative power of the soil. The proposed scheme of sensing has been implemented, which confirmed the feasibility of retrieval of the temperature depth profile. The technique developed in [3] can be used for retrieval of the soil temperature profile by using the remote sensing data and *a priori* estimates of the soil cover reflection coefficient. In this paper, unlike the studies performed by the authors of [3], we examine the possibility of retrieval of the soil temperature profile, and to calculate the reflection coefficient in the radiometry equation, we construct a model that allows for the temperature profile and temperature dependence of the dielectric permittivity of the topsoil, as well as the unevenness of the air–soil interface.

Unlike the studies considered here, the authors of [4] use a physical model of microwave emission with allowance for the reflection coefficient calculated using the topsoil temperature profiles and the temperature dependence of the dielectric permittivity of organic soils, which is typical of the Arctic tundra. Using the approach developed in [4], the authors of [5] retrieved the temperature profile in the Arctic topsoil on the Alaska North Slope based on radiometric data of the SMOS satellite. The use of angular dependences of the brightness temperature, which were observed for the horizontal and vertical polarizations of the electric field at a frequency of 1.4 GHz in the range of angles from 0° to 65°, made it possible to retrieve the depth temperature profile of soil in a layer 16 cm thick with standard deviation from the true value by no more than 5.5°C.

From the analysis of the literature it follows that the topical problem of the possibility of measuring the temperature depth profile in the Arctic tundra soil using the multifrequency microwave radiometer data remains open. In this paper, we propose using radiometric observations at frequencies of 1.4, 6.93, 7.3, and 10.7 GHz to measure the depth temperature profile in the Arctic tundra topsoil. These frequencies are employed in the MIRAS and AMSR2 radiometers which currently operate onboard the SMOS and GCOM-W1 satellites, respectively. The observed values of the brightness temperature will be calculated in terms of a dielectric model of the Arctic tundra soil [6] and a multifrequency semi-empiric model of microwave emission of bare soils, which in this work will be obtained on the basis of experimental data [7]. The observed values of the brightness temperature will be calculated on the basis of the temperature profiles measured by a weather station of the Toolik lake on the Alaska North Slope. The solution of the radiometric equation will be performed with respect to the soil temperature profile in the piecewise-linear approximation.
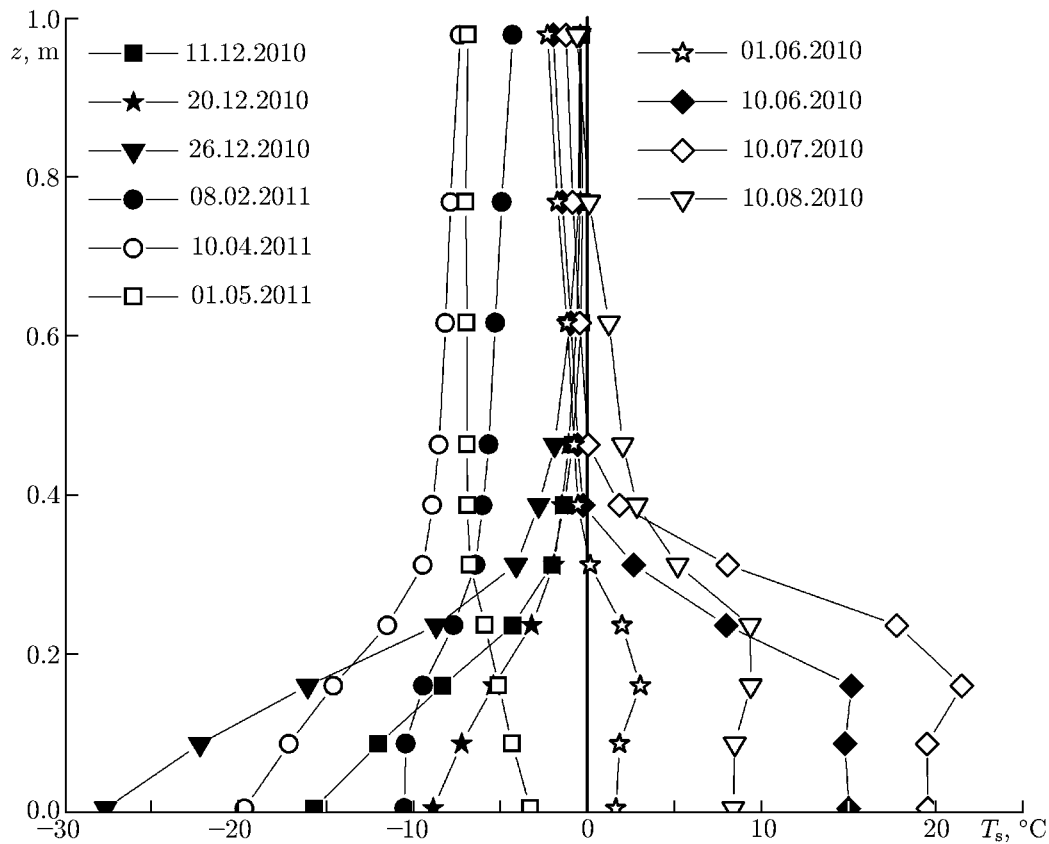
Fig. 1. Typical topsoil temperature profiles measured at the Toolik station during 2010–2011.

2. SURFACE MEASUREMENT DATA ON THE SOIL TEMPERATURE

As the satellite test area, for which the theoretical study was performed, we chose the territory of the Alaska North Slope near the Toolik lake (68.6275° N, 149.5950° W). The choice is due to the fact that in this area we selected the sample soil cover, which served as the basis for a temperature-dependent model of complex dielectric permittivity (CDP) of the soil [6], as well as the fact that detailed profiles of the topsoil temperature and humidity for this area are in open access [8]. The Toolik station measures the daily average soil temperature profiles at depths of 0.6, 8.7, 16.0, 23.6, 31.2, 38.7, 46.3, 61.6, 76.8, and 97.8 cm and soil humidity at depths of 9, 12, 38, 39, and 68 cm [8]. As an example, Fig. 1 shows some depth profiles of the soil temperature $T_s(z)$ belonging to the winter and summer time. It is seen in this figure that in a surface layer 16 cm thick, the temperature dependence on depth is close to linear in the winter time and virtually does not change with the depth in the summer time. The landscape of the test area represents a typical Arctic tundra. The plot is covered with moss and low grasses [9]. The upper horizon of the soil cover 4 to 15 cm thick was formed by organic soils with an average dry density of 0.08 to 0.36 g/cm^3 [10]. The depth of melting of the soil cover reaches 50–70 cm, and the maximum thickness of the snow cover ranges from 20 to 40 cm [9]. In summer, the average volume humidity of a 9 cm surface layer varies only weakly from year to year and is about 0.45.

Based on the data given above, we will use the following approximations to construct the model of microwave emission of the tundra soil covers. Firstly, the soil cover will be represented as a layered half-space, whose CDP is a functional of the soil temperature profile. Secondly, we assume that the soil cover is formed by the organic soils only. Thirdly, we neglect scattering and damping of electromagnetic waves in the snow and vegetation covers. In the next Section we present a model of microwave emission of the soil, which was constructed on the basis of these assumptions.

3. MULTIFREQUENCY MODEL OF THE SOIL MICROWAVE EMISSION

Most generally, microwave emission of plane-layered bare soil covers can be described by using a semi-empiric radiometric equation given by [11]

$$T_{B,p}^{th}[\theta_0, \varepsilon(z)] = \eta_p[\theta_0, \varepsilon(z)]T_{eff}[\theta_0, \varepsilon(z)]. \tag{1}$$

Here,

$$\eta_p[\theta_0, \varepsilon(z)] = 1 - \left\{(1-Q)\,|R_p[\theta_0, \varepsilon(z)]|^2 + Q\,|R_q[\theta_0, \varepsilon(z)]|^2\right\}\exp(-H_r\cos^{N_p}\theta_0), \tag{2}$$

$$T_{eff}[\theta_0, \varepsilon(z)] = \int\limits_0^\infty T_s(z)\frac{k_0\kappa_s[\varepsilon(z)]}{\cos\theta[\theta_0, \varepsilon(z)]}\exp\left\{-\int\limits_0^z \frac{k_0\kappa_s[\varepsilon(z')]}{\cos\theta[\theta_0, \varepsilon(z')]}\,dz'\right\}\,dz, \tag{3}$$

$T_{B,p}^{th}[\theta_0, \varepsilon(z)]$ is the brightness temperature for the vertical ($p = V$, $q = H$) and horizontal ($p = H$, $q = V$) polarizations of the electrical radiation component, respectively, $\varepsilon(z) = \varepsilon[\rho_d, m, T_s(z), f]$ is the relative CDP of the soil, which is a function of the density ρ_d, humidity m, the soil temperature profile $T_s(z)$, and the electromagnetic field frequency f, θ_0 is the brightness-temperature observation angle reckoned from the normal, $\eta_p[\theta_0, \varepsilon(z)]$ is the soil emissivity, $T_{eff}[\theta_0, \varepsilon(z)]$ is the effective temperature of the soil [12], Q is a depolarization parameter that allows for the cross-polarization component, $R_{p,q}[\theta_0, \varepsilon(z)]$ is the coefficient of reflection of a plane electromagnetic wave from the layered medium, H_r is the roughness parameter of the soil surface, N_p is the degree of the angular dependence of the soil surface roughness parameter, $\theta[\theta_0, \varepsilon(z)]$ is the angle between the normal to the wave vector of a plane wave and the z axis in the topsoil at a depth z, $k_0 = 2\pi f/c$ is the wave number of free space, c is the light speed in vacuum, and $\kappa_s[\varepsilon_s(z)] = \text{Im}\sqrt{\varepsilon(z)}$ is the normalized damping coefficient in the topsoil at a depth z.

It is seen in model (1)–(3) that the brightness temperature (1) is a functional of the CDP profile and cannot be calculated analytically in the most general case. In a layered medium, the reflection coefficient in Eq. (2) and functional (3) were found numerically using the iteration technique [13] and the Simpson method [14], respectively. For a numerical calculation of the reflection coefficient and functional (3), the topsoil was divided into n elementary layers, with the boundary coordinates specified in the form of grid nodes $z_1 = 0, \ldots, z_i, \ldots, z_n$ with uniform spacing. The upper limit of integration in improper integral (3) was assigned equal to z_n. The Fresnel reflection coefficient (see Eq. (2)) and functional (3) were calculated with allowance for refraction of the electromagnetic wave in the topsoil, so that in the neighboring elementary layers with the numbers i and $i + 1$, the angles of incidence θ_i and refraction θ_{i+1} of the electromagnetic wave are related by the Snell's law:

$$\cos\theta_{i+1} = \sqrt{1 - (\varepsilon_i/\varepsilon_{i+1})\sin^2\theta_i},$$

where $\theta_{i=1} = \theta_0$. This method of numerical calculation allows for the influence of the temperature-dependent complex dielectric permittivity and the soil temperature, which are inhomogeneous in depth in the topsoil, on the brightness temperature (1).

The connection between the parameters Q, H_r, and N_p in model (1)–(3) and the variance of the soil-cover roughness heights σ and the electromagnetic field frequency f has poorly been studied. Predominantly, these parameters are determined empirically, with minimized residual norm between model (1)–(3) and the experimentally measured brightness temperature [15]. Let us find the connection between the parameters Q, H_r, and N_p and the electromagnetic field frequency and variance of the soil-cover roughness heights by reanalysis of the experimental data given in [7]. The authors of that paper measured the angular dependence of the brightness temperature for the vertical and horizontal polarizations at frequencies of 1.4, 5.0, and 10.7 GHz over the melted bare soil cover, with the variance of the soil-cover surface roughness heights varied from 0.21 to 2.45 cm and different granule-metric composition of the soils. The mass content of lime m_c
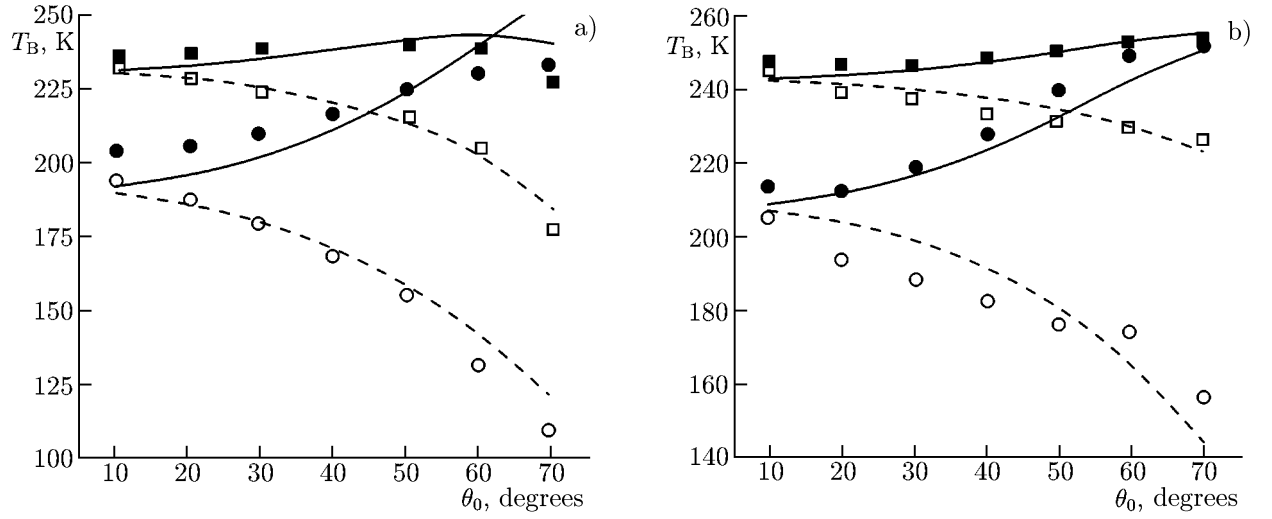
Fig. 2. Angular dependences of the brightness temperature observed at frequencies of 1.4 GHz (a) and 10.7 GHz (b). Filled and open symbols denote the measured values, and solid and dashed lines, calculated values of the brightness temperature for the vertical and horizontal polarizations, respectively. The squares correspond to the variance of the soil surface inhomogeneities $\sigma = 2.45$ cm and the circles, to $\sigma = 0.73$ cm. The soil temperature is $20°$C. The volume humidity of soil is 0.250 and 0.259 for $\sigma = 2.45$ and 0.73 cm, respectively.

varied from 0.14 and 0.25. Some of the measured angular dependences of the brightness temperatures T_B are given in Fig. 2.

To describe the angular dependences of the brightness temperature, which are similar to those shown in Fig. 2 using radiometric equation (1), we make the following assumptions: Firstly, in Eq. (2) we assume that $N_H = N_V = 0$. Secondly, we assume the soil temperature T_s. Then (3) can be written in the form $T_{\text{eff}}(\theta) = T_s$. Thirdly, let the parameters Q and H_r in Eq. (2) be functions of σ and f:

$$Q = a[1 - \exp(-b\sigma f^2)], \qquad H_r = p[1 - \exp(-d\sigma f^2)], \quad (4)$$

where b and d are measured in $\text{cm}^{-1} \cdot \text{GHz}^{-2}$, σ, in cm, and f, in GHz. Parameters a, b, p, and d will be found by minimizing the residual norm between the measured (see Fig. 2) and calculated (using Eqs (1)–(4)) angular dependences of the brightness temperature. The minimization was performed by using the Levenberg–Marquardt algorithm [16]. As a result, we obtain the following optimal values of the parameters: $a = 0.34 \pm 0.12$, $b = 0.60 \pm 0.28$ $\text{cm}^{-1} \cdot \text{GHz}^{-2}$, $p = 0.65 \pm 0.09$, and $d = 0.03 \pm 0.01$ $\text{cm}^{-1} \cdot \text{GHz}^{-2}$. As an example, Fig. 2 shows the angular dependences of the brightness temperature,

Fig. 3. Correlation between the calculated T_B^{Calc} and measured T_B^{Meas} brightness temperatures at frequencies of 1.4, 5.0, and 10.7 GHz in the range of observation angles from $10°$ to $70°$ in the case of a relatively smooth ($\sigma = 0.73$ cm) and rough ($\sigma = 2.45$ cm) soil surface. Filled and open symbols correspond to the vertical and horizontal polarizations, respectively.

which were calculated on the basis of model (1)–(4), in the cases of a relatively smooth ($\sigma = 0.73$ cm) and rough ($\sigma = 2.45$ cm) surface of the soil cover for two frequencies. Note that in the calculation of the brightness temperature in Eqs. (2) and (3), we used the model of a complex dielectric permittivity of mineral soils [17]. The result of the correlation analysis of calculated and experimental values of the brightness tem-
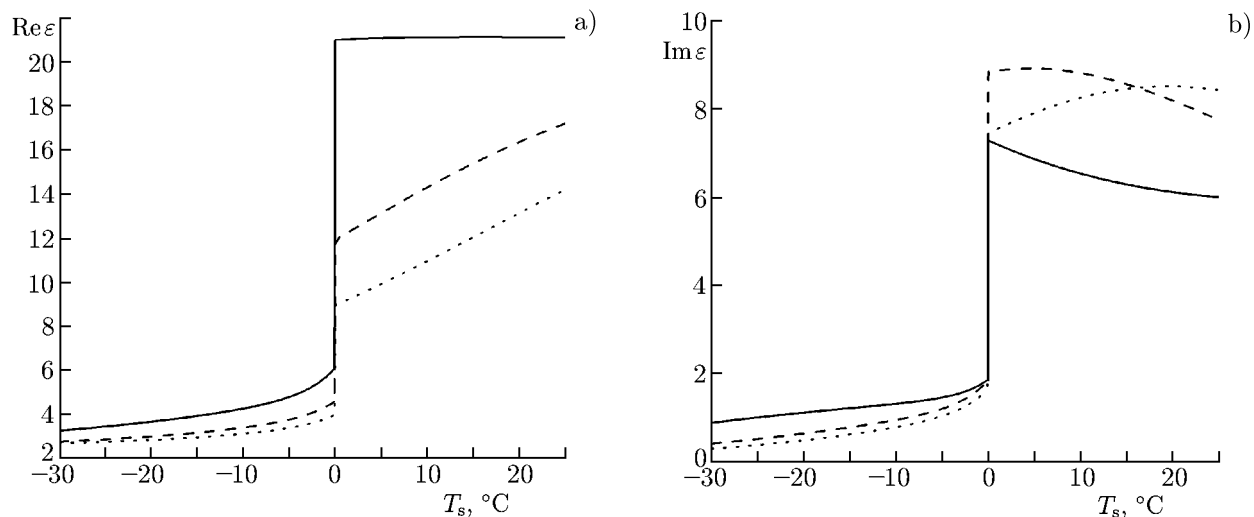
Fig. 4. The real (*a*) and imaginary (*b*) parts of CDP of the soil selected at the Toolik lake, which were calculated on the basis of the model [6]. The solid line corresponds to the frequency $f = 1.4$ GHz, the dashed line, to the frequency $f = 7.3$ GHz, and the dotted line, to the frequency $f = 10.7$ GHz.

perature is presented in Fig. 3. In the case of the horizontal (vertical) polarization, the correlation coefficient and the variance appeared equal to 0.97 (0.89) and 5.8°C (6.3°C).

As a result, we constructed a mathematical model given by Eqs. (1)–(4), which describes the brightness temperature for the horizontal and vertical polarizations of a melted, bare soil cover in a frequency range of 1.4 to 10.7 GHz and for the variance of the soil-cover surface roughness heights varied from 0 to 2.45 cm. We will use this model for calculation of the microwave emission of frozen soils, assuming that the physical temperature variations of the soil will be allowed for due to the temperature-dependent CDP of the Arctic tundra soil in Eqs. (2) and (3) [6], and the found connections (4) will not change significantly. Note that in the previous semi-empiric model [11] of microwave emission at a frequency of 1.4 GHz, which was experimentally substantiated for melted mineral soils with natural humidity variations under field conditions and variance of the soil-cover roughness heights from 5 mm to 6 cm. The depolarization Q and roughness H_r parameters turned out to be independent of the dielectric permittivity and humidity of the soil. The main contribution of the dielectric permittivity and humidity of the soil in mathematical model (1)–(3) is allowed for due to the reflection coefficient and effective temperature of the soil which are included in this model. The CDP model [6] was created on the basis of the soil samples selected at the Toolik station. The soil samples contained 87% of organic substance, 8% of quartz, and 5% of calcite. Model [6] calculates the soil CDP $\varepsilon = \varepsilon_s(\rho_\mathrm{d}, m_g, T, f)$ as a function of the dry density ρ_d, weight humidity m_g ($0.0 \leq m_\mathrm{g} \leq 0.98$), temperature T ($-30\,^\circ C \leq T \leq 25^\circ$C), and frequency f ($0.5 \leq f \leq 15$ GHz). The standard deviation of calculated from measured values of CDP does not exceed 0.17 [6]. Note that the dielectric model [6] was constructed from measurements of the CDP of the soil cover samples during freezing, and the soil sample in the measuring cell got frozen at $-6°$C. In the further modeling, to ensure freezing of the soil at 0°C in the dielectric model [6], the temperature scale was shifted by 6°C. Such an artificial technique admits a relative error in the predicted real and imaginary parts of the CDP by no more than 15% in a temperature range of -10 to 0°C. As an example, Fig. 4 shows the real and imaginary parts of the CDP as functions of temperature and frequency of the electromagnetic field for given dry density and volume humidity of the soil, 0.22 g/cm^3 and 0.45, respectively.

Based on microwave emission model (1)–(4), the CDP model [6], and the temperature profiles measured by the Toolik station and similar to those shown in Fig. 1, we calculate the temperature dependence of the brightness temperature for the vertical and horizontal polarizations at 1.4 and 10.7 GHz from January 1, 2010 to December 31, 2011. The variance of the soil-cover surface roughness heights was assigned
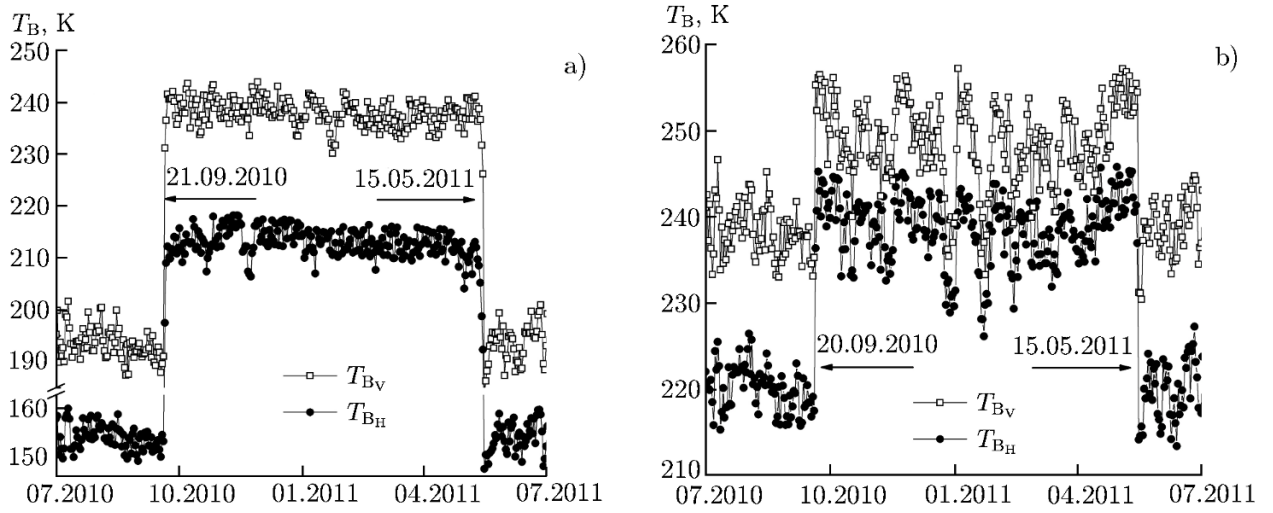
Fig. 5. Dynamics of the brightness temperature of the soil at a frequency of 1.4 GHz (*a*) and 10.7 GHz (*b*) from July 1, 2010 to July 1, 2011. The horizontal axis indicates the month and the year.

equal to $\sigma = 2$ cm. The soil density was assumed equal to its average value $\rho_d = 0.22$ g/cm^3 measured at the Toolik station [10] in the surface layer 20 cm thick. We specify the weight humidity of the soil, $m_g = m_v/\rho_d$, by using the average value of the soil volume humidity $m_v = 0.45$, which was measured at the Toolik station in summer during 2010–2011. In the numerical calculation of the reflection coefficient (see Eq. (2)) and effective temperature (3), the number of elementary layers was assigned equal to $n = 220$. The upper integration limit in the improper integral (3) was taken equal to $z_n = 1$ m. The calculation of the brightness temperature for the horizontal and vertical polarizations was provided with relative error less than 1%, and the number of elementary layers increased from 220 to 240. The obtained time dependences of the brightness temperature are given in Fig. 5.

It is seen from the data presented in Fig. 5 that the freezing (melting) of the soil cover is accompanied with an abrupt increase (decrease) in brightness temperature. It follows from the brightness temperature data at a frequency of 1.4 GHz (see Fig. 5*a*) that the soil became frozen one day later than according to the brightness temperature data at a frequency of 10.7 GHz (see Fig. 5*b*). This can be explained by the fact that the sensing depth at a frequency of 1.4 GHz exceeds the depth of the initially frozen layer of the soil, which is comparable with the sensing depth at a frequency of 10.7 GHz. Consequently, as the freezing front moves into the soil interior, the brightness temperature first experiences a jump at a frequency of 10.7 GHz and then at a frequency of 1.4 GHz.

In the next Section, based on the data presented in Fig. 4, we develop a method for the temperature profile retrieval in the topsoil. The data given in Fig. 5 will serve as initial "measured" values of the soil brightness temperature.

4. THE TEMPERATURE PROFILE RETRIEVAL METHOD

As was mentioned in Sec. 2, the temperature profiles (see Fig. 1) in a soil layer 16 cm thick can be represented in the form of a linear function of depth. As the model of the topsoil temperature profile, we take a piecewise-linear function

$$T_s(z) = \begin{cases} T_0 + T_g z, & z < z_L; \\ T_0 + T_g z_L, & z \geq z_L. \end{cases} \tag{5}$$

Here, T_0 and T_g are the temperature on the soil surface and the temperature gradient in a soil layer of thickness z_L, respectively. Temperature below the point $z = z_L$ is assumed constant and equal to $T_0 + T_g z_L$. In accordance with model (1)–(5), the brightness temperature $T_{B,p}^{th}(\theta)$ can be considered as a function of the

form

$$T_{B,p}^{th}(\theta) = T_{B,p}^{th}(f_i, \theta, \rho_d, m_g, T_0, T_g, z_l, \sigma). \tag{6}$$

The frequencies f_j $(j = 1, \ldots, 4)$ and the observation angle θ of the brightness temperature will be specified by equal quantities typical of the microwave sensing satellites currently operated, namely, $f_1 = 1.4$ GHz (SMOS/MIRAS), $f_2 = 6.93$ GHz, $f_3 = 7.3$ GHz, and $f_4 = 10.7$ GHz (GCOM-W1/AMSR2), and $\theta = 55°$. It follows from the Toolik station data that the average humidity of the soil surface layer 9 cm in summer varies only weakly from year to year. In order to decrease the number of parameters required for the brightness temperature retrieval, according to Eq. (6), we calculate the soil humidity m_g using the average volume humidity of the soil, $m_v = 0.45$ cm^3/cm^3, which was measured at the Toolik station in summer during 2010–2011. We also fix the layer thickness $z_L = 16$ cm of the soil having a temperature gradient. It follows from the weather station data (see Sec. 2 and Fig. 1) that in summer the temperature in a layer 16 cm thick varies with the depth. Based on this approximation, we assume that in summer $T_s(z) = T_s$; then $T_{eff}(\theta) = T_s$. Thus, the following set of parameters in Eq. (6) is subject to retrieval: ρ_d, T_0, T_g, and σ in winter and ρ_d, T_0, and σ in summer. In what follows, we denote the set of these parameters by the vector **p**.

The algorithm of retrieval of the parameters **p** was constructed by minimization of the residual norm between the "measured" $T_{B,p}^m(f_j)$ and calculated $T_{B,p}^{th}(f_j)$ values of the brightness temperature

$$F(\rho_d, T_0, T_g, z_L, \sigma) = \sum_{j=1}^{4} |T_{B_V}^m(f_j) - T_{B_V}^{th}(f_j)|^2 + |T_{B_H}^m(f_j) - T_{B_H}^{th}(f_j)|^2. \tag{7}$$

Functional (7) was minimized using the Levenberg–Marquardt algorithm [16]. As the initial values of the components of the vector **p**, we used $\rho_d = 0.4$ g/cm^3, $T_0 = -10°$C, $T_g = 0$ °S/m, and $\sigma = 0$ cm.

In order to introduce the error observed in the experiment to the simulated initial values of the brightness temperature $T_{B_p}^m(f_j)$, a random quantity with a 2K half-width Gaussian distribution was added to the values $T_{B_p}^m(f_j)$. The chosen noise level corresponds to the claimed error of measurement of the brightness temperature by MIRAS and AMSR2 radiometers onboard the CMOS [18] and GCOM-W1 [19] satellites, respectively.

5. THE RESULTS AND DISCUSSION

The soil temperature at depths of 0.6 and 16 cm, which was measured at the weather station and retrieved on the basis of radiometric data (see Fig. 5), is shown in Fig. 6.

The soil temperature at depths of 0.6 and 16 cm was calculated on the basis of the retrieved parameters T_0 and T_g and Eq. (5). It is seen in Fig. 6 that the retrieved values of the soil temperature at a depth of 0.6 cm better correspond to the measured values than at a depth of 16 cm. Retrieved and measured values of the soil temperature at depths of 0.6 and 16 cm in winter are shown in Figs. 7a and 7b. Retrieved and measured values of the effective soil temperature at a depth of 0.6 cm in summer are given in Fig. 7c.

In order to consider the limiting case, we performed a similar correlation analysis (see Fig. 7) for the noise level 4 K, which exceeds two times the error of measurement of the brightness temperature by the MIRAS and AMSR2 radiometers onboard the SMOS and GCOM-W1 satellites, respectively. The variance and correlation coefficients for the correlation analysis are presented in Table 1.

It is seen in Table 1 that the error of retrieval of the soil temperature at a depth of 16 cm increases about threefold compared with a similar value at a depth of 0.6 cm. As the noise level increases from 2 to 4 K, the error of measurement of the temperature at a depth of 16 cm increases by about two times. In summer, the error of measurement of the soil temperature is more than two times smaller than a similar value in winter. The retrieved dry density of the soil and the variance of the soil surface roughness heights for the winter (summer) time of the year appeared equal to $\rho_d = 0.21 \pm 0.04$ g/cm^3 (0.22 ± 0.02 g/cm^3) and $\sigma = 1.93 \pm 0.26$ cm ($\sigma = 2.01 \pm 0.07$ cm), respectively.
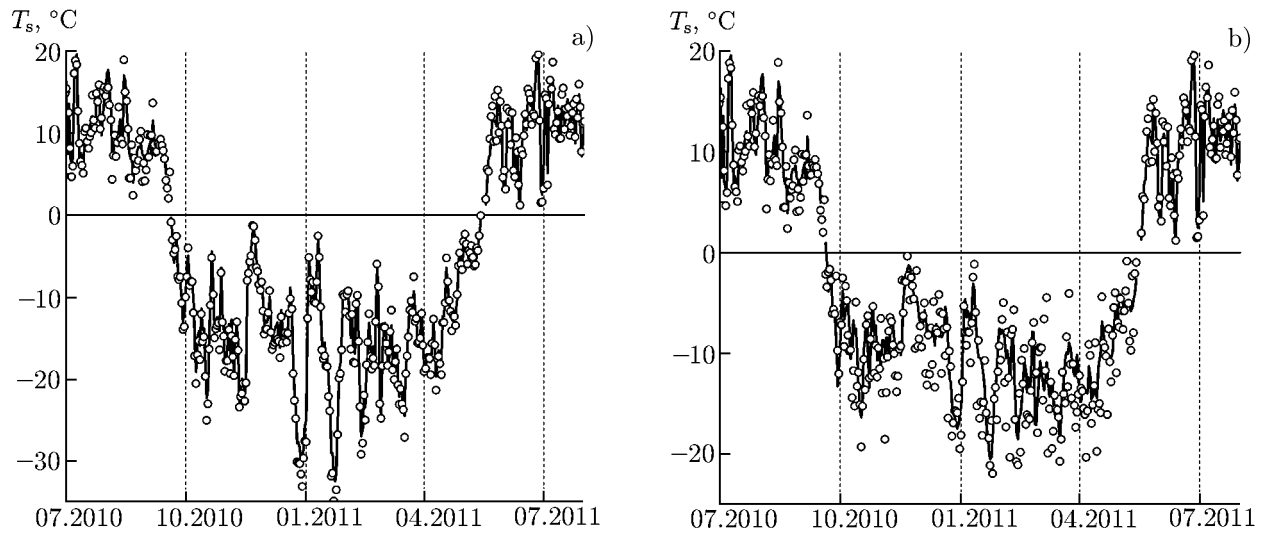
Fig. 6. The soil temperature measured at the Toolik station (solid line) and retrieved from radiometric data (circles) at depths of 0.6 (*a*) and 16 cm (*b*). In summer, the temperature measured at the weather station is given for a depth of 0.6 cm. The horizontal axis indicates the month and the year.

We now compare the errors of measurement of the soil temperature at the noise level 4 K and the errors we observed in the experiment [2] on the Happy Valley test area that is the nearest to the Toolik station. In [2], the variance of retrieved soil temperatures from the values measured by the weather station in a layer 5 cm thick varied from 5.53 to 9.23°C and from 3.2 to 5.0°C for the winter and summer times, respectively. The corresponding correlation coefficient was 0.48–0.5 in winter and 0.76–0.77 in summer. Compared with [2], the method proposed in this paper predicts temperature in the soil surface layer at a depth of 0.6 cm with a factor of four better accuracy and gives a similar dry error at a depth of 16 cm (see Table 1). The error of retrieval of the soil temperature on the basis of the multifrequency method (SMOS+GCOM-W1) proposed in this paper is comparable with the error of the single-frequency method (SMOS) proposed in [4, 5]. Since the SMOS satellite is designed to shoot the Arctic regions up to three times a day and the GCOM-W1 satellite, up to four times a day, the combined use of the data from these satellites can permit space monitoring of the diurnal dynamics of the depth soil temperature profiles.

The method proposed in this paper did not allow for the following factors, whose effect on the soil temperature retrieval error should be studied elsewhere. When sensing from space, the pixel of a radiometric shot has an average size of about 43×43 km, within the limits of which the Earth's surface is inhomogeneous relative to vegetation and soil covers (organic and mineral soils) and may contain open water areas. In this regard, it remains unclear what effect the above features of the soil surface have on the soil temperature retrieval error. The influence of the snow and vegetation covers on the temperature retrieval error for the soil during freezing and melting also needs additional study. Moreover, the created model of microwave emission needs to be modified, since it does not allow for the inhomogeneous distribution of the soil humidity in depth and the layered structure of the upper (organic) and lower (mineral) horizons in the active topsoil, which is typical of the Arctic tundra. The influence of the humidity profile, as well as of the mineral horizon in the active topsoil on the soil measurement error, also requires more research.

6. CONCLUSIONS

In this theoretical paper, we propose a method for measuring the depth temperature profile of the active topsoil of the Arctic tundra on the basis of the brightness observations in a frequency range of 1.4 to 10.7 GHz for the vertical and horizontal polarizations. The proposed approach is specific in that it offers the combined use of spectral physical models of microwave emission of the soil cover and the temperature-

347
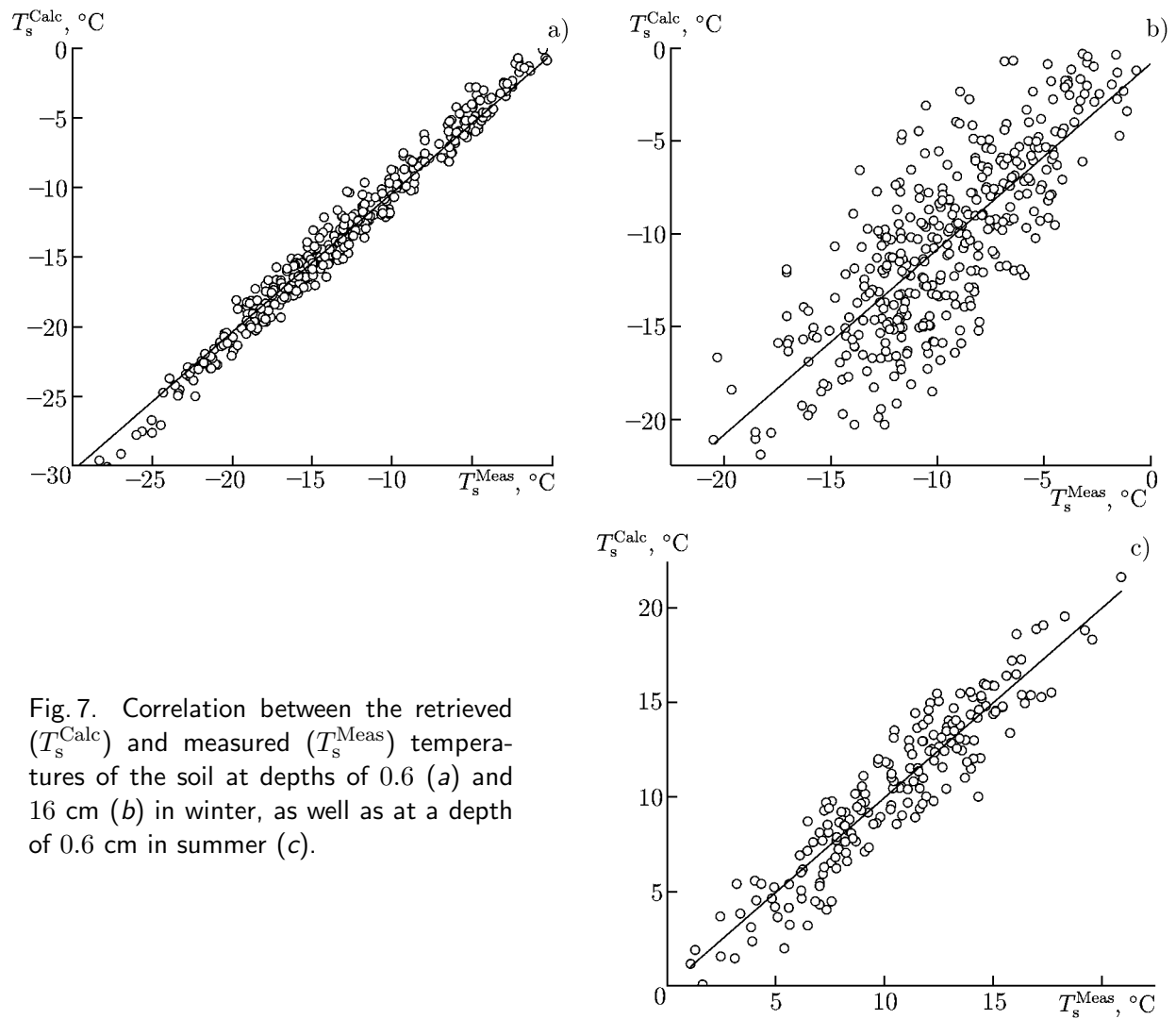
Fig. 7. Correlation between the retrieved (T_s^{Calc}) and measured (T_s^{Meas}) temperatures of the soil at depths of 0.6 (*a*) and 16 cm (*b*) in winter, as well as at a depth of 0.6 cm in summer (*c*).

TABLE 1. The soil temperature retrieval error in the winter (summer) time.

Depth, cm	Noise level 2 K		Noise level 4 K	
	Variance, $^\circ C$	Correlation coefficient	Variance, $^\circ C$	Correlation coefficient
0.6	1.1 (1.5)	0.98 (0.88)	2.3 (4.4)	0.89 (0.48)
16.0	3.2 (−)	0.62 (−)	7.2 (−)	0.22 (−)

dependent complex dielectric permittivity of the Arctic tundra soil. This method correctly allowed for the effect of the temperature gradient and relative complex dielectric permittivity in the active topsoil (at depths of 0 to 16 cm) on the microwave emission of the frozen soil cover. The variance in the temperature measurement varied from 1.1 to 2.3°C and from 3.2 to 7.2°C with the noise level increased from 2 to 4 K, respectively. The corresponding correlation coefficient varied from 0.89 to 0.98 and from 0.22 to 0.62. In summer, the error of measurement of the soil temperature is two times smaller compared with the winter time. With allowance for the high periodicity of the space shooting by the SMOS and GCOM-W1 satellites at the Arctic latitudes (up to 3–4 times a day), the created method can be the basis for monitoring of the

diurnal dynamics of the temperature mode of the Arctic tundra soils. For the further testing of the method proposed in this paper we will use the actual satellite data of SMOS and GCOM-W1 for the satellite test areas of the Yamal Peninsula and the Alaska North Slope. We plan to explore the influence of the inhomogeneity of the soil cover (organic and mineral soils) and the soil humidity, both on the surface and deep in the soil, of the vegetation and snow covers, as well as of the open water areas, on the soil temperature measurement error.

REFERENCES

1. S. Hachem, C. R. Duguay, and M. Allard, *Cryosphere*, **6**, No. 1, 51 (2012).

2. L. A. Jones, J. S. Kimball, K. C. McDonald, et al., *IEEE Trans. Geosci. Remote Sens.*, **45**, No. 7, 2004 (2007).

3. K. P. Gaikovich, A. N. Reznik, and R. V. Troitsky, *Radiophys. Quantum Electron.*, **32**, No. 12, 1082 (1989).

4. V. L. Mironov, K. V. Muzalevskiy, and I. V. Savin, *IEEE J. Selected Topics Appl. Earth Observat. Remote Sens.*, **6**, No. 3, 1781 (2013).

5. K. V. Muzalevskiy and V. L. Mironov, *Izv. Vyssh. Uchebn. Zaved., Fizika*, **56**, No. 10/3, 88 (2013).

6. V. L. Mironov, R. D. De Roo, and I. V. Savin, *IEEE Trans. Geosci. Remote Sens.*, **48**, No. 6, 2544 (2010).

7. J. R. Wang, P. E. O'Neill, T. J. Jackson, et al., *IEEE Trans. Geosci. Remote Sens.*, **GE-21**, No. 1, 44 (1983).

8. http://www.nrcs.usda.gov/wps/portal/nrcs/detail/soils/home/?cid=NRCS142P2_053712 .

9. P. F. Sullivan, M. Sommerkorn, H. M. Rueth, et al., *Oecologia*, **153**, 643 (2007).

10. http://www.geobotany.org/library/reports/BarredaJE2006_daltonhwy_20060301.pdf .

11. J. P. Wigneron, Y. H. Kerr, P. Waldteufel, et al., *Remote Sens. Environment*, **107**, 639 (2007).

12. M. Schwank, K. Rautiainen, C. Mätzler, et al., *Remote Sens. Environment*, **154**, 180 (2014).

13. L. M. Brekhovskikh, *Waves in the Layered Media*, Academic Press, New York (1973).

14. B. P. Demidovich and I. A. Maron, *Numerical Methods of Analysis* [in Russian], Nauka, Moscow (1966).

15. H. Lawrence, J.-P. Wigneron, F. Demontoux, et al., *IEEE Trans. Geosci. Remote Sens.*, **51**, No. 7, 4075 (2013).

16. G. H. Golub and C. F. van Loan, *Matrix Computations. 3rd edition*, Johns Hopkins University Press, Baltimore and London (1996).

17. V. L. Mironov, L. G. Kosolapova, and S. V. Fomin, *IEEE Trans. Geosci. Remote Sens.*, **47**, No. 7, 2059 (2009).

18. S. Pinori, R. Crapolicchio, and S. Mecklenburg, in: *Microwave Radiometry and Remote Sensing of the Environment, Firenze, 11–14 March 2008*, p. 1.

19. M. Kachi, K. Naoki, and M. Hori, in: *Int. Geosci. Remote Sens. Symp., Munich, 21–26 July 2013*, p. 831.